

A Soft-Rigid Air-Propelled Pipe-Climbing Robot

Qingxiang Zhao*, Zhiyi Jiang*, and Henry K. Chu[†], Member IEEE

Abstract—Complex pipeline network should be inspected regularly for safety. In general, these tasks are often completed by large pipe-climbing robots or customized equipment. Most of them are not effective, and cannot work on pipes with uncertain barriers. Moreover, some pipes are mounted in constrained scenarios, so bulky robots are not applicable. This paper presents a tethered soft-rigid pipe-climbing robot to fill the gap. Two indispensable actions, i.e. embracing pipe and moving along it, are realized by a soft component and a 3D printed wheel mechanism. The latter includes two forces: thrust force from the compressed air and tractive force from wheels, to drive the robot comprehensively, and a lightweight body (only 160g) benefits agile motion. In operation, pressure exerted on the soft component enables the robot to embrace pipes of different diameters, with controllable adhesion force, and locomotion force is also regulated. Inspired from vehicle, an elastic damper is attached between the wheel structure and the robot body, which can effectively alleviate vibration when crossing barriers. In addition, theoretical models are constructed to analyse and control thrust force, and the locomotion performance is analysed by dynamics model. Experiments demonstrate that this robot can perform rapid climbing at a speed of 1.09m/s in load-free scenarios, and it can move at a maximum speed of 0.828m/s with 500g load. Reconstruction of a flexible pipe using the robot is also demonstrated.

I. INTRODUCTION

Pipeline is widely applied in energy industry, chemical engineering, and metallurgy, and the structural health is highly related to safety. Therefore, performing regular health detection for the pipes is valuable and necessary, such as monitoring rust degree, and detecting inner defection of steel pipe with magnetic transducer or ultrasonic sensor. Currently, these tasks are often completed manually or by dedicated apparatus, with low level of automation. Furthermore, pipeline is often mounted in a constrained environment, where human labour cannot reach. It is valuable to develop robots that can travel along the pipe surface with built-in detection tools to replace manual intervention with high effectiveness. The climbing behaviour is shown in Fig. 1, where two factors are generally needed: embracing pipe (adhesion force), and forward or backward locomotion actions along it (locomotion force).

First, to generate adhesion force, a typical solution is employing vacuum cups [1]–[3]. A cone-shaped cup connecting to a vacuum pump that can provide negative air pressure adheres to-be-climbed object’s surface, and stronger

Qingxiang Zhao, Zhiyi Jiang, and Henry K. Chu are with the Department of Mechanical Engineering, Hong Kong Polytechnic University, Hong Kong, China.*These authors contributed equally to this work. [†]Corresponding author, email: henry.chu@polyu.edu.hk

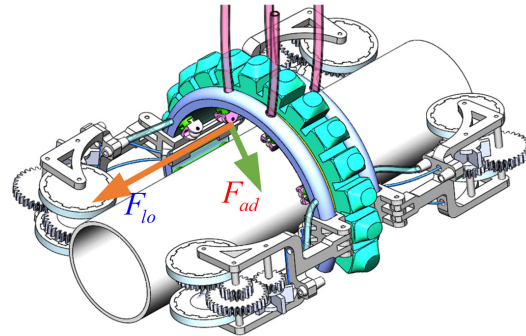


Fig. 1. Illustration of pipe-climbing robot. Adhesion force F_{ad} and locomotion force F_{lo} are required to achieve pipe climbing task.

negative pressure leads to bigger adhesion force. For example, inspired by inchworm behaviour, Guan *et al.* [3] developed a rigid wall-climbing robot using negative pressure to stabilize the robot. The shortcoming of this method is that the touching surface between vacuum cup and to-be-climbed objects should be clean and flat, as proper sealing is required to avoid pressure leakage. Actuating artificial muscle with high voltage deforms elastomer and embedding metal foil inside it could generate adhesion force. This method was applied by Gu *et al.* [4] who proposed a wall climbing robot, where two electro-adhesive feet are periodically controlled to walk on a flat wall, but a high voltage (6KV) is needed. To adapt different configurations of to-be-climbed objects, soft structure is a good alternative, and its deformation degree is often regulated by fluids or cables [5], [6]. The deformation state is regulated sequentially and periodically, but hysteresis of soft material leaves difficulty to return its rest state rapidly, leading to limited motion velocity and even obvious fluctuation. Similar to extensible elastomer, the length of Shape Memory Alloy (SMA) coil [7], [8] can be controlled by the material temperature, but it often needs complicated electronic circuits. Heating and cooling are both time-consuming, which inherently influences locomotion velocity. In addition to these flexible structures, classical ‘spring pressing apparatus’ provides a normal force [9] perpendicular to the pipe surface, but it has marginal ability to adapt different pipes. Also, the bulky body makes it difficult to work in a constrained space. A magnet mounted at the bottom of a robot can prevent it from dropping when climbing metal pipes [10]. However, plastic pipes that commonly used in industries and some environments are magnetism forbidden,

which invalidates this adhesion force. Learning from animals' climbing, previous studies found that Van der Waals' force [11] and wet adhesion (based on capillary effects) [12] can also provide adhesion force. Nevertheless, some prerequisites about touching surface should be fulfilled, and the adhesion force is complicated to control. In this paper, a totally flexible structure is employed to embrace pipe physically, without requirement material of pipes, and the deformation degree of it is involved in embracing force.

In addition to adhesion, robot should also be able to move along a pipeline, namely locomotion force is needed. This force that is the principal motion of robot, relates to climbing velocity. Most existing works adopted compliant property of elastomer, which can be lengthen [6] or shorten [13] upon actuated by fluids [14] or electric energy [15]. Mckenna *et al.* [16] developed a snake-like robot using propulsive force from robot skin, whose shortcoming may be that the robot is only able to perform single-direction motion. Wheel-type climbing robot [17] can move along a pipeline by rotating wheels along the pipe direction. It relies on adhesion force heavily to generate static friction force, and the full rigid components make it cumbersome. Climbing actions learned from animals stimulate multi-legged walking mode. Aracil *et al.* [18] presented a parallel climbing robot. By changing the length of parallel pods, robot can climb along pipes; however, it requires complicated hardware to sense the length of pods and synchronization algorithm to ensure smooth progress. Similarly, Shimada *et al.* [19] developed a climbing robot based on human climbing behaviour, which should grasp the wall/pipe tightly. Using electro-adhesive feet, SMA material [8] has also been applied to drive robots. Furthermore, a quadrupedal robot developed by Clark *et al.* [20] can rapidly climb a pole with embracing actions. These climbing ways are often highly coupled with adhesion behaviour, and the robot can only perform periodical actions. This may not be practical in inspection/detection since vibration should be refrained ensuring smooth work of precise detection tools.

Most of the aforementioned solutions are with slow climbing velocity or cannot travel within a confined space, and some cannot climb pipes with different diameters or specific pipe material. This is often caused by hysteresis of material, bulky body and actuation mechanism. Analysing existing works, we found that although adhesion and locomotion are both necessary, they sometimes conflict with each other. As stronger adhesion force improves robustness, it increases friction between the robot and the pipe surface, finally decreasing the climbing velocity. Therefore, an ideal pipe-climbing robot should be: 1) lightweight, 2) agile locomotion, 3) work with a large range of pipe diameter, and 4) work in diverse conditions. This paper presents a soft-rigid pipe-climbing robot, in which the adhesion action is realized by inflating air into an unsymmetrical elastomer structure, and the locomotion force is achieved using air propulsion and wheel-driven mechanism. The two actions are decoupled so that control scheme could be individually designed. The main contributions of this work include:

- ◊ The full compliance property of soft robotics is applied to

adapt different pipes.

- ◊ Using hybrid force to drive robot.
- ◊ Investigating the control model of robot.
- ◊ Demonstrating one potential application.

The rest of this paper is organized as follows. Section II describes the setup of this robot. Fundamental analysis and control model are included in Section III. Experimental results are detailed in Section IV. Section V concludes this work.

II. PLATFORM

In this section, the design and fabrication procedures of our robot are detailed, and illustrated in the first part of supplementary video. In brief, this hybrid robot has two modules: compliant embracing module (*CEM*) and locomotion component (*LC*). Details of their fabrication processes are illustrated in Fig. 2(a).

A. Design of CEM

Soft material has a higher degree of flexibility and can adapt a wide range of pipe's diameter. We adopt a curve structure (made of silicon) to embrace pipe, and due to unsymmetrical structure, it can be deformed like an arch upon pressurized. As shown in Fig. 2(a) (I)-(III), both the hump layer and the bottom layer are fabricated using mold and cast. An inextensible TPU thin film is bonded below the bottom layer to promote easier bending. Two rows of rollers are configured beneath the TPU film to transfer sliding friction into rolling friction while climbing, enabling the robot to cross barriers on pipe surface. Besides, stronger embracing force will not influence locomotion significantly because of rolling friction.

B. Design of LC

The locomotion component should generate sufficient locomotion force to drive robot moving along the pipe. Inspired by rocket that is actuated by thrust force of compressed high-temperature gas, we also utilize this method to provide energy for robot. As shown in Fig. 2(a) (V), a tube is connected to a nozzle that is mounted on the frame of a gear ratio mechanism, and once high-speed air is ejected from the outlet of the nozzle, reaction thrust force F_t occurs. There are two nozzles on the frame, from which the compressed air can rotate wheel clockwise and counter-clockwise, respectively, so as to move robot forward and backward. The thrust cannot leverage the full energy of the compressed air, with lots of kinetic energy left. Therefore, a fan blade is attached behind the nozzle to collect the remaining energy, which can rotate the fan with a high angular velocity. The fan rotates one gear and torque is amplified by the gear ratio mechanism (with the ratio of 4:1), which acts as a speed reducer. The surface of the wheel is encapsulated by silicon rubber, similar to the tire of car's wheel, to avoid slippage. Consequently, tractive force F_f also actuates the robot to move along the pipe. The four gear ratio mechanisms can be separately controlled, so that forward and backward locomotions can both be achieved.

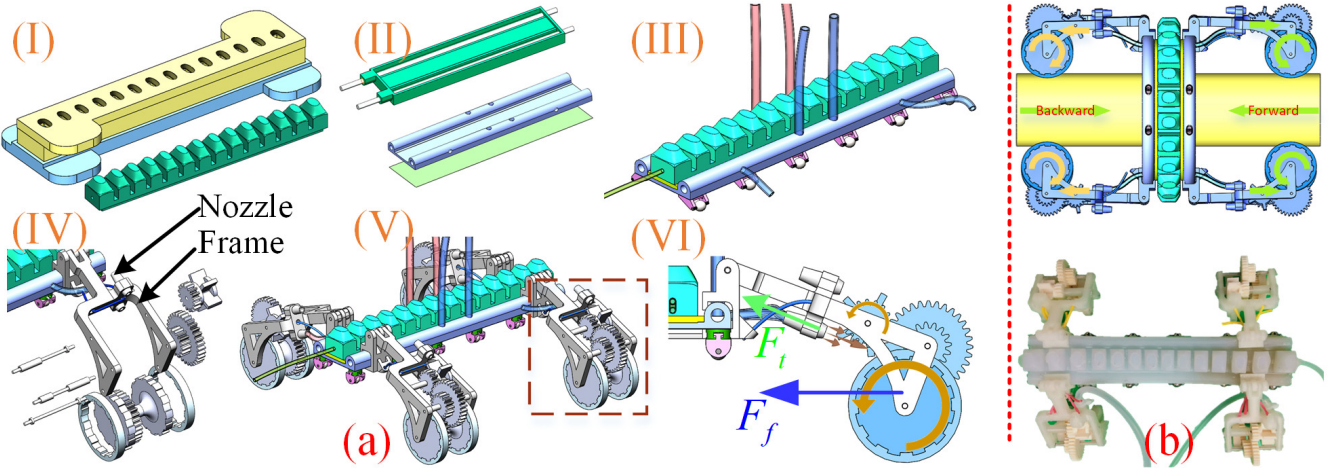


Fig. 2. Fabrication process and overview of the robot. (a) Illustration of fabricating *CEM* and *LC*. (I) Pour silicon rubber into a 3D printed mold to get a hump layer. (II) Fabricate a flat bottom layer and attach a TPU film beneath it. (III) Bond the hump layer, the bottom layer and other attachments, forming compliant embracing module (*CEM*). (IV) Print frame and gears, and assemble gear ratio mechanism. (V) Four gear ratio mechanisms are assembled on *CEM*. (VI) An illustration of *LC* and its actuation principle. (b) Working principle and snapshot.

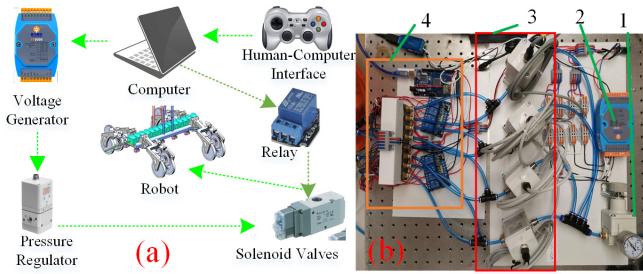


Fig. 3. Implementation hardware setup. (a) Operation flowchart among hardware. (b) Experiment setup. 1-Inlet pressure gauge, 2-Analogue voltage generator, 3-Pneumatic pressure regulators, and 4-Solenoid valves are prepared for changing direction.

C. Implementation Setup

Since the energy of this robot is purely provided by compressed air and the performance depends on air pressure, the hardware to regulate it should be well designed. As illustrated in Fig. 3(b), four (one for backup) pneumatic pressure regulators (FESTO VPPE-3-1-1) are commanded to control air pressure, among which one is for embracing behaviour and others are for locomotion. Fig. 3(a) shows the operation flow of robot system. A joystick (Logitech Gamepad F710) acts as human-computer interface, and computer controls pneumatic pressure via analogue voltage generator. Solenoid valves are selectively actuated by relays, to change the direction of locomotion.

III. MODELS

In this section, we investigate the adhesion behaviour, i.e. mapping between pressure and deformation, and build dynamics model involved in locomotion.

A. Pressure-Deformation Model

When embracing circular pipes, the air pressure should be properly set, otherwise too small pressure can not embrace pipe and too strong pressure generates exceeded adhesion force. The shape of *CEM* is assumed as an arch, whose radius is required to generally follow the diameter of to-be-climbed pipe, so a mapping between inflating pressure P_a and radius R is investigated. The flexibility of material, complex structure, and fabrication imperfections, all throw challenges to find an explicit mapping, so statistics method is a simple but effective alternative. Herein, a cubical non-linear regression algorithm is used, to fit the mapping, which is:

$$R = W \underbrace{\begin{bmatrix} p_a^3 & p_a^2 & p_a & 1 \end{bmatrix}}_X^T \quad (1)$$

where $W \in R^{1 \times 3}$ is a parametrized matrix that can be solved by:

$$W = (X^T X)^{-1} X^T R \quad (2)$$

We use a well calibrated RGB-D camera (Intel Realsense D415) to measure the radius of the pressurized robot, and the radius extraction process is shown in Fig. 4(a). For each given pressure, six points located at the TPU film is extracted from RGB image and corresponding depth distance information is obtained via depth image. Using the position of the six points, we approximate the deformed TPU film as a circle. The setting pressure varies from 0.02 bar to 0.18 bar, and the radius of each approximated circle is plotted in Fig. 4(b), where the fitted mapping results using (1) is also included. It can be observed that the algorithm can estimate the radius properly and the error is small. Especially, within the frequently-used pressure range: 0.12-0.18 bar, the error is negligible. Theoretically, this pressure can only help to embrace pipe without exerting a strong adhesion force, which

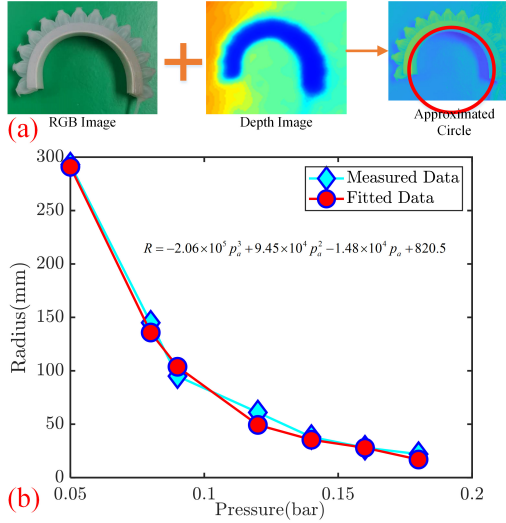


Fig. 4. Illustration of radius extraction and fitting process. (a) Fuse RGB-D information to extract deformation radius of the CEM. (b) Comparison between the true radii (measured by RGB-D camera) and the fitted ones.

is indispensable since the locomotion behaviour is mainly from wheels. The actual pressure is selected by adding 0.03 bar to the required pressure calculated via (1), namely $\tilde{P}_a = P_a + 0.03$, to ensure that proper normal force between wheels and pipe surface exists.

B. Locomotion Model

As displayed in Fig. 2(a) (V) and Fig. 5(a), the components of the locomotion has two parts: 1) Thrust force F_t from compressed air and 2) Tractive force F_f from wheels, so the resultant locomotion force is :

$$F_{lo} = F_t \cos(\theta) + 2F_f \quad (3)$$

where θ is the angle between the frame and the pipe. If the angle between the pipe and the horizontal plane is α , the acceleration a is:

$$a = [F_{lo} - G \sin(\alpha) - \mu(G \cos(\alpha) + N)]/m \quad (4)$$

where μ is rolling frictional coefficient, G is gravity, m is the mass of robot, and N is the normal force between robot and pipe surface except that from gravity.

1) Model of Thrust Force

We assume the air flow inside nozzle is an isentropic quasi-one-dimension flow, which is shown in Fig. 5(b), such that the thrust force F_t can be calculated by:

$$F_t = \dot{m}v_e + (p_e - p_\infty)A_e \quad (5)$$

where \dot{m} is mass flow rate, A_e is the area of nozzle's outlet. The mass flow rate is obtained by: $\dot{m} = \rho_e v_e A_e$. To calculate it, we assume the temperature inside the nozzle is room temperature $25^\circ C$, value of specific gas constant $R = 287 J/(kgK)$, and the effective ratio of specific heat

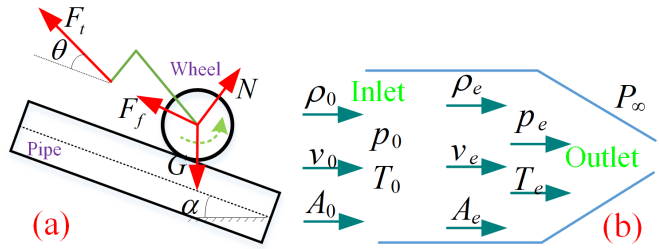


Fig. 5. (a) Force analysis of gear ratio mechanism. (b) Cross section of nozzle, in which compressed air flows from left to right. ρ_0 and ρ_e are density of air, v_0 and v_e are velocity, p_0 and p_e are air pressure, and T_0 and T_e are temperature, at inlet and outlet respectively. P_∞ is barometric pressure.

$\gamma = 1.4$. Therefore, the density ρ_e , temperature T_e at outlet, and velocity v_e can be computed via:

$$\begin{aligned} \rho_e &= \frac{p_0}{RT_0} \left(\frac{2}{\gamma + 1} \right)^{\frac{1}{\gamma-1}} \\ T_e &= \left(\frac{2}{\gamma + 1} \right) T_0 \\ v_e &= \sqrt{\gamma RT_e} \end{aligned} \quad (6)$$

2) Model of Tractive Force

The remaining kinetic energy from the compressed air directly exerts on the fan, and the rotating fan further transmits rotation movement toward to the encapsulated wheel via a gear ratio mechanism whose ratio is 4:1. Let T_w denote the torque of one wheel, which can be calculated by:

$$T_w = 4F_t \eta_f \eta_g^2 R_w \quad (7)$$

where η_f is the efficiency of thrust force, and η_g is the transmission efficiency of the two-stage gear ratio mechanism. Assume there is no slippage phenomenon between wheel and pipe surface, such that the angular velocity ω of the wheel can be solved by Newton's second law:

$$\begin{aligned} J \frac{d\omega}{dt} &= T_w - F_f R_w \\ F_f &= \mu N \end{aligned} \quad (8)$$

where J is the rotational inertia of wheel, and R_w is wheel's radius.

IV. EXPERIMENTS

To validate the proposed methods and test the performance of the robot, several experiments are conducted.

A. Thrust Force Validation

A nozzle with the same dimension as that mounted on the frame is fabricated to validate the model of thrust force. The nozzle is fixed and the air flowing through it is ejected towards a scale to directly measure the thrust force (see Fig. 6(a)). The pressure is regulated from 0 bar to 6 bar with an increment of 0.5 bar, and the measured force and the theoretical are illustrated in Fig 6(b). Theoretically, the thrust force is linear with the air pressure, but the actual data is non-linear

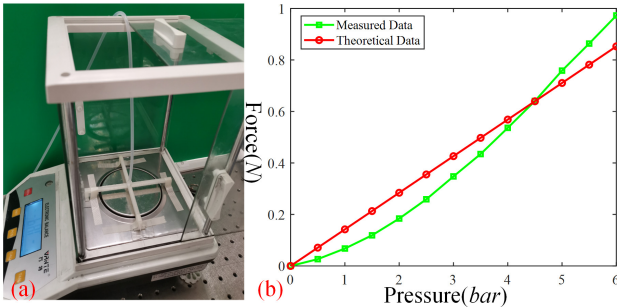


Fig. 6. (a) Thrust force measurement setup. (b) Comparison between the measured thrust force and the theoretical.

with the increment of it. The similar increasing trend proves that the proposed aerodynamics model can provide reference to design scheme. The reason behind this phenomenon is that the flow rate will slightly increase with the increase of air pressure, leading to the mass flow rate improved, while the air flow rate in (5) is assumed as constant. In addition, when the air pressure is relatively small, the ejected air spreads towards ambient direction more, such that the force exerted on the scale is smaller than the theoretical analysis.

B. Locomotion Force Validation

In addition to measuring the thrust force, the resultant locomotion force is also verified. Robot is commanded to embrace the pipe with different air pressures that exceeds the minimum value calculated by (1) to avoid falling. Three PVC pipes with diameter of 32mm, 40mm, and 50mm, are utilized for testing. Behind the robot, a digital force meter (SF-100, Sanliang Corp.) is fixed, and a Nylon thread connecting the robot to the force meter through a series of fixed pulleys. Fig. 7(b) shows the three conditions. Then, air pressure ranging from 0 to 5.2 bar is applied on robot, and Fig. 7(a) plots the corresponding locomotion force under different settings. It can be observed that the robot is almost immobile when the pressure is below 2 bar, which means the robot should overcome static friction force before climbing. Air is not ejected directly to the fan but dissipated to the surroundings as the pressure is too small. For a same pipe, a stronger P_a leads to bigger F_{lo} due to that the wheel has bigger normal force with the pipe surface. Increasing the pipe diameter essentially decreases θ , such that the thrust force increases. Therefore, the locomotion force on the middle size pipe is bigger than the smallest one. Besides, the total length of the CEM is 155mm, and the circumference of the three pipes are: 100.48mm, 125.6mm, and 157mm, respectively. This proves that our robot is capable of climbing pipes whose diameters varies largely with reference to its body length.

C. Dynamic Performance

Since the above experiments have proven this robot can embrace different pipes and locomotion force is obviously observed, dynamic performance deserves to be investigated.

1) Typical free climbing movements

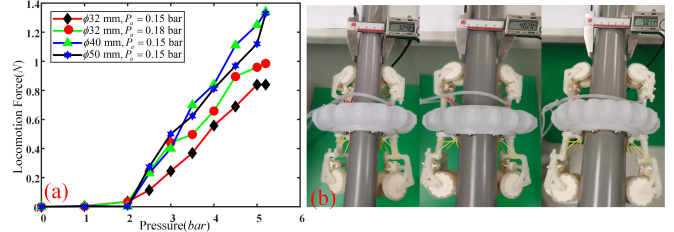


Fig. 7. (a) Illustration of measured resultant locomotion force when robot is climbing different size of pipe, and the exerted air pressure starts from 0 to 5.2 bar. (b) Robot is working on three pipes whose diameters are 32mm, 40mm, and 50mm (from left to right).

Deformation of CEM and motion of wheels are recorded in second part of the supplementary video, demonstrating the embracing behaviour and locomotion are both well controlled.

Three pipes are horizontally placed to test the typical climbing performance. The embracing pressure is set to 0.14 bar, and the unique variable is driving pressure p_0 , which is respectively set to 3, 4 and 5 bar for comparison (the minimal pressure to actuate robot is around 2.3 bar). As displayed in video, the velocity difference is not obvious when same p_0 applied on the different pipes, but robot moves faster with increased p_0 . The length of each pipe is limited to only 80cm, so robot cannot accelerate to its maximum velocity. At the end point, robot knocks towards a foam board, and the impact forces vary sharply for the three diverse locomotion setting. One of the nine climbing scenarios is displayed in Fig. 8(a). As shown in Fig. 8(b), the maximum mean velocity is 1.3m/s, which is excellent compared with other climbing counterparts.

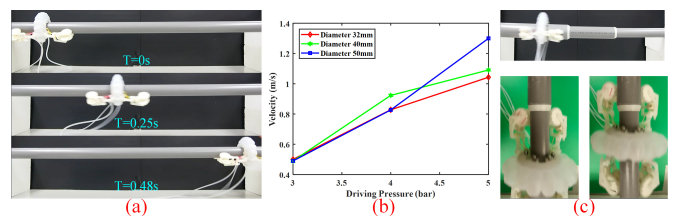


Fig. 8. (a) Snapshots of climbing pipe (pipe diameter is 40mm and driving pressure is 4bar). (b) Mean velocity comparison. (c) Illustration of climbing diameter-changeable pipe, including before and after crossing barrier.

2) Barrier-crossing performance

A pipe with multiple diameters is considered to examine the barrier-crossing performance of this robot. The three pipes are serially connected. When robot moves from left to right, it encounters a larger resistance from the section with a larger diameter, and vice versa. Results show that in whichever condition, it can still robustly embrace the pipe and continue to locomote, which means the damper structure functions well. The barrier-crossing process is included in

the fourth part of video and Fig. 8(c).

3) On-load climbing

Its load carrying ability is also tested. Robot is commanded to climb 40mm-diameter pipe and the locomotion pressure is 5 bar. Load with 200g, 400g, and 500g are respectively hang at the bottom of robot, and the corresponding mean velocities are: 0.828m/s, 0.511m/s, and 0.453m/s. This proves that our robot is capable of performing on-load climbing task, and it can carry at least load with three times of its body weight. The climbing processes are also included in the fourth part of the video.

4) Shape reconstruction for a flexible pipe

Since this robot can carry considerable load in locomotion, it can also finish pipe-related tasks carrying proper tools. Therefore, a shape reconstruction task for flexible pipe is considered, where robot is set to embrace a pipe (foam pipe coated with Nylon net, with diameter of 48mm). A tracking system (Flex 13, OptiTrack) is employed to find the position of three markers that are mounted on robot, and the whole setup is displayed in Fig. 9(a). To ensure the markers are always visible for the tracker, the gear ratio mechanism is detached, and robot starts from the higher end of the pipe such that the energy provided purely by thrust force is sufficient. The scanning process and results are respectively demonstrated in the fifth part of the video and Fig. 9(b). A little vibration is observed at the starting stage, due to the need of a larger force to overcome static force, which however does not affect the whole shape of the flexible pipe.

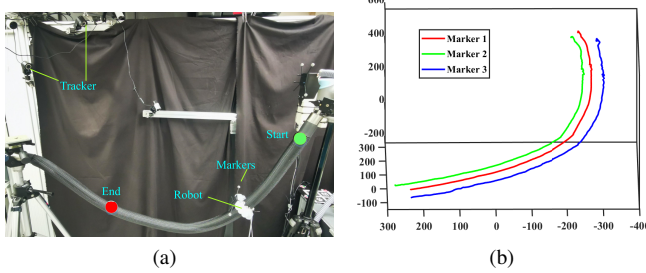


Fig. 9. Flexible pipe shape scanning. (a)Experimental setup. (b)Trajectory of three markers.

V. CONCLUSION

This paper presents a tethered soft-rigid pipe climbing robot that can travel outside a pipe effectively. The soft component enables the robot to adapt pipes with different diameters. Compressed air provides power for adhesion and locomotion. Due to thrust force of air and kinetic energy collection mechanism (the gear ratio mechanism), the locomotion velocity is enhanced greatly. This is a clean energy such that robot can work in many scenarios like magnetic-free, underwater environments. In theory, increased ratio of the gear ratio mechanism will enhance the resultant locomotion force.

REFERENCES

- [1] A. Kanada, F. Giardina, T. Howison, T. Mashimo, and F. Iida, "Reachability improvement of a climbing robot based on large deformations induced by tri-tube soft actuators," *Soft robotics*, vol. 6, no. 4, pp. 483–494, 2019.
- [2] J.-G. Lee and H. Rodrigue, "Origami-based vacuum pneumatic artificial muscles with large contraction ratios," *Soft robotics*, vol. 6, no. 1, pp. 109–117, 2019.
- [3] Y. Guan, H. Zhu, W. Wu, X. Zhou, L. Jiang, C. Cai, L. Zhang, and H. Zhang, "A modular biped wall-climbing robot with high mobility and manipulating function," *IEEE/ASME transactions on mechatronics*, vol. 18, no. 6, pp. 1787–1798, 2012.
- [4] G. Gu, J. Zou, R. Zhao, X. Zhao, and X. Zhu, "Soft wall-climbing robots," *Science Robotics*, vol. 3, no. 25, 2018.
- [5] A. Sadeghi, A. Mondini, E. Del Dottore, A. K. Mishra, and B. Mazzolai, "soft-legged wheel-based robot with terrestrial locomotion abilities," *Frontiers in Robotics and AI*, vol. 3, p. 73, 2016.
- [6] G. Singh, S. Patiballa, X. Zhang, and G. Krishnan, "A pipe-climbing soft robot," in *2019 International Conference on Robotics and Automation (ICRA)*. IEEE, 2019, pp. 8450–8456.
- [7] J.-S. Koh and K.-J. Cho, "Omegabot: Crawling robot inspired by ascotis selenaria," in *2010 IEEE International Conference on Robotics and Automation*. IEEE, 2010, pp. 109–114.
- [8] Q. Wu, V. Pradeep, and X. Liu, "A paper-based wall-climbing robot enabled by electrostatic adhesion," in *2018 IEEE International Conference on Soft Robotics (RoboSoft)*. IEEE, 2018, pp. 315–320.
- [9] O. Unver and M. Sitti, "Tankbot: A palm-size, tank-like climbing robot using soft elastomer adhesive treads," *The International Journal of Robotics Research*, vol. 29, no. 14, pp. 1761–1777, 2010.
- [10] M. Tavakoli, C. Viegas, L. Marques, J. N. Pires, and A. T. De Almeida, "Omniclimbers: Omni-directional magnetic wheeled climbing robots for inspection of ferromagnetic structures," *Robotics and Autonomous Systems*, vol. 61, no. 9, pp. 997–1007, 2013.
- [11] K. Autumn, Y. A. Liang, S. T. Hsieh, W. Zesch, W. P. Chan, T. W. Kenny, R. Fearing, and R. J. Full, "Adhesive force of a single gecko foot-hair," *Nature*, vol. 405, no. 6787, pp. 681–685, 2000.
- [12] W. Federle, M. Riehle, A. S. Curtis, and R. J. Full, "An integrative study of insect adhesion: mechanics and wet adhesion of pretarsal pads in ants," *Integrative and Comparative Biology*, vol. 42, no. 6, pp. 1100–1106, 2002.
- [13] T. Manwell, T. Vitek, T. Ranzani, A. Menciassi, K. Althoefer, and H. Liu, "Elastic mesh braided worm robot for locomotive endoscopy," in *2014 36th Annual International Conference of the IEEE Engineering in Medicine and Biology Society*. IEEE, 2014, pp. 848–851.
- [14] B. Liao, H. Zang, M. Chen, Y. Wang, X. Lang, N. Zhu, Z. Yang, and Y. Yi, "Soft rod-climbing robot inspired by winding locomotion of snake," *Soft Robotics*, 2020.
- [15] Q. He, Z. Wang, Y. Wang, A. Minori, M. T. Tolley, and S. Cai, "Electrically controlled liquid crystal elastomer-based soft tubular actuator with multimodal actuation," *Science advances*, vol. 5, no. 10, p. eaax5746, 2019.
- [16] J. C. McKenna, D. J. Anhalt, F. M. Bronson, H. B. Brown, M. Schwerin, E. Shammas, and H. Choset, "Toroidal skin drive for snake robot locomotion," in *2008 IEEE International Conference on Robotics and Automation*. IEEE, 2008, pp. 1150–1155.
- [17] Y. Liu, S. Sun, X. Wu, and T. Mei, "A wheeled wall-climbing robot with bio-inspired spine mechanisms," *Journal of Bionic Engineering*, vol. 12, no. 1, pp. 17–28, 2015.
- [18] R. Aracil, R. J. Saltaren, and O. Reinoso, "A climbing parallel robot: a robot to climb along tubular and metallic structures," *IEEE Robotics & Automation Magazine*, vol. 13, no. 1, pp. 16–22, 2006.
- [19] A. Shimada and N. A. Dung, "Equilibrium state control for climbing robot," in *2016 IEEE 14th International Workshop on Advanced Motion Control (AMC)*. IEEE, 2016, pp. 455–460.
- [20] G. C. Haynes, A. Khripin, G. Lynch, J. Amory, A. Saunders, A. A. Rizzi, and D. E. Koditschek, "Rapid pole climbing with a quadrupedal robot," in *2009 IEEE International Conference on Robotics and Automation*. IEEE, 2009, pp. 2767–2772.